

Enhanced neutrino signals from dark matter annihilation in the Sun via metastable mediators

Nicole F. Bell and Kalliopi Petraki

School of Physics, The University of Melbourne, Victoria 3010, Australia

E-mail: n.bell@unimelb.edu.au, kpetraki@unimelb.edu.au

Abstract. We calculate the neutrino signal resulting from annihilation of secluded dark matter in the Sun. In this class of models, dark matter annihilates first into metastable mediators, which subsequently decay into Standard Model particles. If the mediators are long lived, they will propagate out from the dense solar core before decaying. High energy neutrinos undergo absorption in the Sun. In the standard scenario in which neutrinos are produced directly in the centre of the Sun, absorption is relevant for $E \gtrsim 100$ GeV, resulting in a significant suppression of the neutrino spectrum beyond $E \sim 1$ TeV. In the secluded dark matter scenario, the neutrino signal is greatly enhanced because neutrinos are injected away from the core, at lower density. Since the solar density falls exponentially with radius, metastable mediators have a significant effect on the neutrino flux, even for decay lengths which are small compared to the solar radius. Moreover, since neutrino detection cross sections grow with energy, this enhancement of the high energy region of the neutrino spectrum would have a large effect on overall event rates.

Contents

1	Introduction	1
2	Neutrino production and propagation in the Sun	2
2.1	Injection from mediator decay	4
2.2	Interactions	4
2.2.1	Neutral-current interactions	4
2.2.2	Charged-current interactions	5
2.3	Flavour oscillations	6
2.3.1	$\nu_e - \nu_\mu$ oscillations	6
2.3.2	$\nu_\mu - \nu_\tau$ oscillations	8
2.4	Propagation	9
3	Neutrino signals	11
3.1	Neutrino flux results	11
3.2	Muon event rates	16
4	Conclusions	17

1 Introduction

The gravitational capture and subsequent annihilation of dark matter (DM) in the Sun offers a compelling possibility for DM detection. DM particles passing through the Sun are expected to scatter off nuclei, lose energy, and become trapped by the gravitational field. Multiple scatterings cause DM to sink towards the centre of the Sun. If DM self-annihilates, the capture is quickly balanced by the annihilation of DM particles. The intensity of the annihilation signal is then a probe of the DM scattering cross section on nucleons [1, 2]. Signals from DM capture in the Sun (or the Earth) are expected to be detectable in the future. Standard Model (SM) particles other than neutrinos, produced in the annihilations, interact strongly with the interior of the Sun and are largely absorbed. In this process though, they produce high-energy neutrinos which escape, and can be potentially seen by neutrino detectors, such as IceCube and DeepCore. Extensive studies of the expected neutrino signal from DM annihilation via various SM channels have been performed, in a model-independent way [3, 4], and for particular models [5–20]. Limits from Super-Kamiokande and IceCube on annihilation of WIMP and Kaluza-Klein DM in the Sun and the Earth have been reported in Refs. [21–23].

It is possible, however, that DM does not annihilate directly into SM particles, but rather into metastable mediators which subsequently decay into SM states, $\chi\chi \rightarrow VV \rightarrow \text{SM}$, as recently discussed in [24–29]. In such models, the thermal relic WIMP DM scenario can be realised as usual, while there is also the potential to explain astrophysical observations, e.g. the positron excess observed by PAMELA [26, 27]. The seclusion of DM from the SM, which in this class of models communicate only via metastable mediators, can dramatically change the annihilation signature of DM captured in the Sun. For example, if the mediators are sufficiently long-lived to escape the Sun before decaying, they can produce detectable charged-particle or γ -ray fluxes, as discussed in Refs. [30, 31].

If the mediators are short-lived and decay in the interior of the Sun, energetic neutrinos remain the only signature. However, even for decay of V inside the Sun, the neutrino signal can be dramatically enhanced compared to the standard scenario. This is because high energy neutrinos can interact with nuclei and be absorbed before escaping the Sun. In the standard scenario, in which neutrinos are produced at the centre of the Sun, the neutrino energy spectrum is damped as $e^{-E_\nu/\mathcal{E}}$, with a critical energy of $\mathcal{E} \sim 100$ GeV. However, the solar density decreases exponentially with radius, so if neutrinos are injected by V decay at larger radii they are subject to much less absorption as they propagate out of the Sun. We thus expect the critical energy scale for absorption to increase exponentially with the neutrino injection radius, increasing rapidly once the injection point is moved outside the dense core.

For simplicity, we will consider the case where the mediators, V , decay directly to neutrinos $V \rightarrow \nu\bar{\nu}$, as this will suffice to illustrate the difference between DM annihilations with and without mediators. It is of course plausible that the mediators decay to other SM model particles, which subsequently produce energetic neutrinos. Although we shall not study this case in detail, we note that greatly enhanced signals are also expected in this scenario. For instance, if DM annihilates directly to light quarks or muons at the centre of the Sun, the neutrino yield is negligible, as these particles quickly lose energy and are absorbed before they can decay to produce neutrinos. However, if a mediator decay were to inject light quarks or muons at radii beyond the dense core, then a non-negligible neutrino flux would result; absorption effects are of course completely avoided if the decay occurs outside the solar radius [30].

In this paper, we consider the neutrino signal at the Earth from annihilation of secluded DM in the Sun, for a range of mediator lifetimes and DM masses. In Sec. 2 we describe the production of neutrinos from decay of the mediator, review the relevant aspects of neutrino interactions in the Sun, namely absorption, regeneration, and flavour evolution. We also describe the numerical approach we follow to calculate the neutrino signal at the Earth. Our main results are presented in Figs 4 – 8. In Sec. 3 we discuss the results, and compare them with the standard case of DM annihilation directly into SM particles.

2 Neutrino production and propagation in the Sun

During the capture and thermalisation of dark matter in the Sun, the DM particles undergo multiple scatterings and become concentrated within a rather small region of size $\sim 0.01R_\odot\sqrt{100\text{ GeV}/m_\chi}$ around the centre of the Sun, where R_\odot is the solar radius. The finite size of this region has a negligible effect on the final neutrino spectra [1, 3, 4], and thus the DM annihilations can be assumed to take place in the centre of the Sun.

In the scenario considered here, DM annihilates into metastable mediators

$$\chi\chi \rightarrow VV, \tag{2.1}$$

which subsequently decay into neutrino pairs

$$V \rightarrow \nu\bar{\nu}. \tag{2.2}$$

The mediators are emitted with Lorentz factor $\gamma = m_\chi/m_V$. In the rest frame of the Sun, the neutrinos produced from mediator decay uniformly span the energy interval

$$\frac{1}{2}(1 - \beta) m_\chi \leq E_\nu \leq \frac{1}{2}(1 + \beta) m_\chi, \tag{2.3}$$

where β is the mediator velocity, and have an angular dispersion $\delta\theta \sim 1/\gamma$ around the momentum axis of the mediator [30]. As long as $\gamma \gg 1$, the neutrinos are effectively emitted radially outwards, with energies $E_\nu \lesssim m_\chi$. This allows us to use 1-dimensional evolution equations, similarly to the approach commonly adopted in the standard scenario of DM decay directly into SM particles [3, 4, 6].

We will focus on DM masses $100 \text{ GeV} \lesssim m_\chi \lesssim 10 \text{ TeV}$. Neutrinos of energies lower than 100 GeV have negligible interactions in the interior of the Sun, and their final spectrum is not very different from their spectrum at production. At $E_\nu \gtrsim 1 \text{ TeV}$, the absorption of neutrinos in the Sun becomes quite severe, strongly suppressing the signal if neutrinos are injected in the centre of the Sun, as is the case for the standard scenario of DM annihilation directly into SM particles. However, if DM annihilates into metastable mediators, which travel some distance before decaying, the neutrinos transverse smaller optical depth in the Sun and are thus absorbed less. As we shall see, this can change the total flux and spectral shape of the signal for any DM mass $m_\chi \gtrsim 100 \text{ GeV}$, and more dramatically so for $m_\chi \gtrsim 1 \text{ TeV}$.

Once neutrinos are produced, they undergo charged and neutral current scattering with nuclear matter in the Sun, which results in both absorption of high energy neutrinos, and re-injection of neutrinos at lower energy. They also undergo flavour oscillations. For the energy range of interest, the neutrino flavour oscillations and their scattering interactions decouple. The matter potential in the Sun ensures negligible mixing between ν_e and ν_μ, ν_τ until the point of the MSW resonance. For $5 \text{ GeV} \lesssim E_\nu \lesssim 10 \text{ TeV}$, which encompasses our energy range of interest, the resonance occurs after interactions have become unimportant, as will be shown in Sec. 2.3. (Neutrinos below 5 GeV make an insignificant contribution to the signals we consider.) On the other hand, ν_μ and ν_τ mix maximally, with oscillation length typically smaller or comparable to the interaction length. It is then a good approximation to assume that oscillations rapidly equidistribute the ν_μ and ν_τ fluxes, and thus identify their densities and average over their interactions.

The above considerations allow us to follow the evolution of the flavour eigenstates individually, rather than using the full multi-flavour density-matrix formalism. The evolution equations have the form

$$\frac{\partial \rho_j}{\partial r} = \frac{\partial \rho_j}{\partial r} \Big|_{\text{inj}} + \frac{\partial \rho_j}{\partial r} \Big|_{\text{NC}} + \frac{\partial \rho_j}{\partial r} \Big|_{\text{CC}}, \quad (2.4)$$

where $\rho(r, E)dE$ is the neutrino flux, and $j = e$ or μ, τ , for the electron and the averaged muon and tau neutrino fluxes respectively. Similar equations hold for the antineutrinos. The first term on the right-hand side corresponds to the neutrino injection from the mediator decay. The second and the third terms describe the neutrino scattering due to neutral-current (NC) and charged-current (CC) interactions. Neutrino-neutrino scatterings are unimportant, since the neutrino densities are small, and thus the evolution equations remain linear. Each term in Eq.(2.4) is described in detail in the following subsections.

In calculating the neutrino propagation inside the Sun, we adopt the solar nucleon and electron density profiles from the Standard Solar Model [32]. For $r \lesssim 0.9R_\odot$, the nucleon density can be well approximated by

$$N_S(r) \simeq N_0 e^{-\frac{r}{\kappa R_\odot}}, \quad (2.5)$$

with $N_0 = 1.3 \times 10^{26} \text{ cm}^{-3}$ and $\kappa = 0.1$. It will be useful to define the dimensionless optical

depth (independently of the approximation of Eq. (2.5)):

$$x(r) \equiv \frac{1}{N_0 \kappa R_\odot} \int_0^r N_S(r') dr', \quad (2.6)$$

which can be inverted to give $r(x)$. For the region of validity of Eq. (2.5), we obtain the analytic expressions

$$x_a(r) = 1 - e^{-\frac{r}{\kappa R_\odot}}, \quad r_a(x) = \kappa R_\odot \ln \left(\frac{1}{1-x} \right). \quad (2.7)$$

2.1 Injection from mediator decay

Neutrinos are injected by the decay of the metastable mediators produced in the DM annihilations in the center of the Sun, as described in Eqs. (2.1), (2.2). In the steady state regime, the annihilation balances the DM capture in the Sun, $\Gamma_{\text{ann}} = C_\odot/2$, where the capture rate is approximately [2, 5]

$$C_\odot \sim 10^{21} \text{ s}^{-1} \left(\frac{100 \text{ GeV}}{m_\chi} \right) \left(\frac{\sigma_{\text{sc}}}{10^{-42} \text{ cm}^2} \right). \quad (2.8)$$

We will assume that the mediators decay with equal branching ratio to each of the three neutrino flavours $\text{BR}_\nu \equiv \text{BR}_{e,\mu,\tau}$. In the rest frame of the Sun, the neutrino energy spectrum per V decay is flat, $f(E)dE = (\text{BR}_\nu/\beta m_\chi)dE$, for $(1-\beta)/2 \leq E/m_\chi \leq (1+\beta)/2$. The neutrino injection rate is then

$$\left. \frac{\partial \rho(r, E)}{\partial r} \right|_{\text{inj}} = \frac{C_\odot \text{BR}_\nu}{\beta m_\chi} \frac{1}{\beta \gamma \tau} \exp \left(-\frac{r}{\beta \gamma \tau} \right). \quad (2.9)$$

We take the lifetime, τ , of the mediators to be a free parameter, subject only to the big bang nucleosynthesis (BBN) constraint, $\tau < 1 \text{ s}$ [29]. In order to disentangle our results from any astrophysical uncertainties and model-dependence, we shall present our results for the neutrino fluxes normalized to the product $C_\odot \text{BR}_\nu$.

2.2 Interactions

Neutrinos in the Sun interact with the nuclei via neutral and charged currents. The interaction cross sections are rather insensitive to the proton to neutron ratio inside the sun, which varies from 2 in the center, to 7 in the outer regions. We thus adopt the constant value $p/n = 3$ throughout. Scattering on electrons is suppressed in comparison to scattering on nuclei by the ratio of the electron to nucleon mass, m_e/m_N , and we will thus ignore it in this analysis.

2.2.1 Neutral-current interactions

The NC scatterings $\nu_l N \rightarrow \nu_l N$ and $\bar{\nu}_l N \rightarrow \bar{\nu}_l N$ shift the neutrino distributions towards lower energies. The process can be described as removal of a neutrino from the flux and re-injection at a lower energy, as follows

$$\left. \frac{\partial \rho}{\partial r} \right|_{\text{NC}} = N_S(r) \left[-\sigma_{\text{NC}}(E) \rho(r, E) + \int_E^\infty dE' \left. \frac{d\sigma_{\text{NC}}}{dE} \right|_{E' \rightarrow E} \rho(r, E') \right], \quad (2.10)$$

where $N_S(r)$ is the nucleon density of the Sun. The differential and total NC cross sections at the energy range of interest have the form [3, 6, 33]

$$\left. \frac{d\sigma_{\text{NC}}}{dE} \right|_{E' \rightarrow E} = \frac{2G_F^2 m_N}{\pi} [a + b(E/E')^2], \quad (2.11)$$

$$\sigma_{\text{NC}}(E) = \frac{2G_F^2 m_N}{\pi} (a + b/3)E. \quad (2.12)$$

NC scattering is flavour-blind, with

$$\begin{aligned} a_\nu &\simeq 0.06; \quad b_\nu \simeq 0.02; \\ a_{\bar{\nu}} &= b_\nu; \quad b_{\bar{\nu}} = a_\nu. \end{aligned} \quad (2.13)$$

2.2.2 Charged-current interactions

CC interactions convert a neutrino to an almost collinear charged lepton, $\nu_l N \rightarrow l^- N'$ and $\bar{\nu}_l N \rightarrow l^+ N'$. For electron-type neutrinos, this corresponds to removal of a neutrino from the flux. Muon-type neutrinos produce μ^\mp which decay and re-inject neutrinos in the flux, but not before they have thermalised in the plasma and lost most of their energy. The re-injected neutrinos with energies $\sim \text{few} \times 10 \text{ MeV}$ do not contribute to the high-energy neutrino signature of DM annihilations, and for this purpose muon neutrinos that interact via CC are considered absorbed.

Charged-current interactions of ν_τ and $\bar{\nu}_\tau$ produce τ^\mp leptons which decay promptly, before losing their energy, and re-inject energetic neutrinos in the flux. Besides re-injecting a tau-flavour neutrino at a lower energy, the leptonic decays $\tau^- \rightarrow X \nu_\tau$ ($\tau^+ \rightarrow X \bar{\nu}_\tau$) also produce a $\bar{\nu}_e$ (ν_e) 17.8% of the time, and a $\bar{\nu}_\mu$ (ν_μ) 17.4% of the time. (The τ^\mp decay hadronically with probability 64.8%.) Since the contribution to the $\bar{\nu}_e$ (ν_e) and $\bar{\nu}_\mu$ (ν_μ) fluxes from ν_τ ($\bar{\nu}_\tau$) regeneration is suppressed by the branching fraction ~ 0.18 , we will ignore this effect¹. This stands in agreement with similar neutrino signal calculations in various environments which have shown that such a contribution is not significant [34].

The CC absorption and regeneration is described by

$$\left. \frac{\partial \rho_l}{\partial r} \right|_{\text{CC}} = N_S(r) \left[-\rho_l(r, E) \sigma_{\text{CC}}(E) + \int_E^\infty dE' \rho_l(r, E') f_{l \rightarrow l}(E, E') \right]. \quad (2.14)$$

The CC inelastic scattering cross section does not depend on the neutrino flavour, as long as we ignore the effect of the τ mass. This is a good approximation since the τ mass is significant only for $E \lesssim 100 \text{ GeV}$, and at those energies the neutrino interactions in the Sun are unimportant. The CC cross section is [3, 6, 33, 35]

$$\sigma_{\text{CC}}(E) = \frac{2G_F^2 m_N}{\pi} cE, \quad (2.15)$$

with

$$c_\nu \simeq 0.19, \quad c_{\bar{\nu}} \simeq 0.13. \quad (2.16)$$

For the electron and muon flavours we set $f_{l \rightarrow l} \rightarrow 0$, as discussed above. For tau neutrinos these functions encode the appropriate convolution of τ^\mp spectrum arising from CC $\nu_\tau, \bar{\nu}_\tau$

¹As with absorption, regeneration has a smaller effect in the mediator scenario compared to the standard scenario, so this is an even better approximation than usual.

interactions, with the regenerated $\nu_\tau, \bar{\nu}_\tau$ spectrum from the τ^\mp decay. They depend only mildly on the incident neutrino energy, and are merely functions of the ratio of the outgoing to incident neutrino energy, E/E' . We thus adopt the form of $f_{\tau \rightarrow \tau}(E/E')$ and $f_{\bar{\tau} \rightarrow \bar{\tau}}(E/E')$ as presented e.g. in Ref. [3] for incident energy $E' = 400$ GeV.

As will become clear in Sec. 2.4, the neutrino total interaction strength inside the Sun can be conveniently gauged in comparison to the energy scale

$$\mathcal{E} \equiv \left[\frac{2G_F^2 m_N}{\pi} (a + b/3 + c) N_0 \kappa R_\odot \right]^{-1}. \quad (2.17)$$

Using Eqs. (2.13) and (2.16), for neutrinos and antineutrinos respectively, we have

$$\mathcal{E}_\nu \simeq 140 \text{ GeV}; \quad \mathcal{E}_{\bar{\nu}} \simeq 213 \text{ GeV}. \quad (2.18)$$

The values of \mathcal{E} in Eq.(2.18) indicate the approximate energy scale at which interactions become a significant effect and illustrate that absorption is relevant at lower energies for neutrinos than antineutrinos. In terms of \mathcal{E} , the neutrino total interaction cross section becomes

$$\sigma_{\text{tot}}(E) = \frac{1}{N_0 \kappa R_\odot} \frac{E}{\mathcal{E}}. \quad (2.19)$$

The neutrino mean free path, λ_f , defined by

$$\int_r^{r+\lambda_f} \sigma_{\text{tot}}(E) N_S(r') dr' = 1,$$

corresponds to optical depth

$$\delta x_f = \mathcal{E}/E, \quad (2.20)$$

and the neutrino interaction probability is

$$P_{\text{int}} = \int_r^{R_\odot} \sigma_{\text{tot}}(E) N_S(r') dr' = \frac{E}{\mathcal{E}} (x_\odot - x), \quad (2.21)$$

where $x_\odot \simeq 0.9975$ is the optical depth at $r = R_\odot$. In Fig. 1, we sketch the interaction probability contours $P_{\text{int}} = 1$ and $P_{\text{int}} = 0.05$, on the E vs r plane.

2.3 Flavour oscillations

2.3.1 $\nu_e - \nu_\mu$ oscillations

In the inner region of the Sun, the neutrinos experience a matter potential (or refractive index) which aligns the flavour eigenstates with (effective) mass eigenstates, and suppresses oscillations between electron and mu/tau neutrinos. At lower densities, as the matter potential decreases, the e–mu/tau mixing angle increases and the neutrinos go through an MSW resonance. The point of resonance occurs when

$$\frac{\Delta m_{21}^2}{2E} \simeq \sqrt{2} G_F N_e(r), \quad (2.22)$$

where $N_e(r)$ is the electron density profile of the Sun. The radius at which the resonance takes place is shown in Fig. 1. While low energy solar neutrinos go through this resonance adiabatically, remaining in a given mass eigenstate, non-adiabatic effects (in which neutrinos

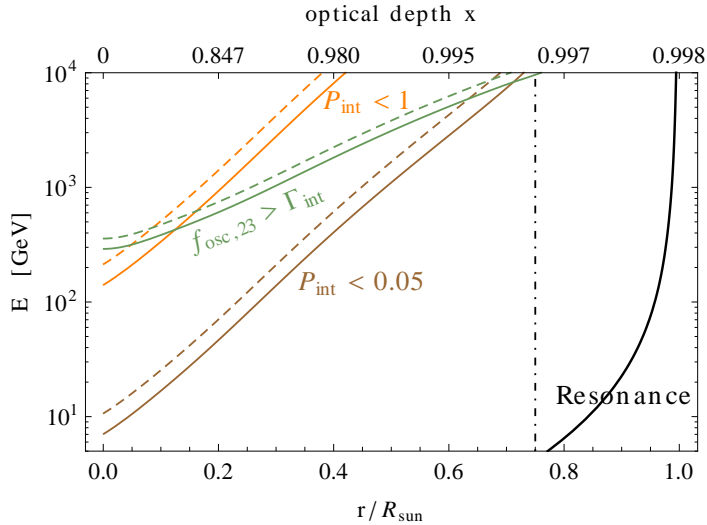


Figure 1. Interaction probability contours, $P_{\text{int}} = 1$ (orange) and $P_{\text{int}} = 0.05$ (brown), for neutrinos (solid lines) and antineutrinos (dashed lines). The black line marks the point of the $\nu_e - \nu_{\mu,\tau}$ resonance. For the energy range of interest, interactions have effectively ceased when neutrinos undergo resonance. We neglect interactions beyond the benchmark point $r_c = 0.75R_\odot$ (dot-dashed line). Oscillations between muon and tau neutrinos occur faster than interactions for energies below the green lines. Neutrinos are then equidistributed between the two flavour eigenstates.

may flip to the other mass eigenstate) are important for neutrinos with energies greater than several ~ 10 GeV. The level-crossing probability at the point of resonance $r = r_{\text{res}}(E)$ is (see e.g. [36])

$$P_C(E) \simeq \frac{e^{\tilde{\gamma} \cos^2 \theta_{12}} - 1}{e^{\tilde{\gamma}} - 1}, \quad \tilde{\gamma}(E) = \frac{\pi r_0 \Delta m_{21}^2}{E}, \quad (2.23)$$

where

$$r_0 = \left| \frac{d \ln N_e}{dr} \right|_{r=r_{\text{res}}(E)}^{-1}, \quad (2.24)$$

while for antineutrinos

$$\bar{P}_C = P_C [\theta_{12} \rightarrow \pi/2 - \theta_{12}]. \quad (2.25)$$

The crossing probabilities $P_C(E)$ and $\bar{P}_C(E)$ are shown in Fig. 2; they become approximately constant for $E \gtrsim 100$ GeV.

After resonance, the fluxes of the three mass eigenstates are

$$\begin{aligned} \rho_1 &= \rho_e^{(i)} P_C + \rho_{\mu,\tau}^{(i)} (1 - P_C), \\ \rho_2 &= \rho_e^{(i)} (1 - P_C) + \rho_{\mu,\tau}^{(i)} P_C, \\ \rho_3 &= \rho_{\mu,\tau}^{(i)}, \end{aligned} \quad (2.26)$$

where $\rho_e^{(i)}(E)$, $\rho_{\mu,\tau}^{(i)}(E)$ are the ν_e and averaged $\nu_{\mu-\nu_\tau}$ fluxes evaluated at the point of resonance, and similarly for the antineutrinos. We convert the mass-eigenstate into flavour-eigenstates fluxes using the standard neutrino mixing matrix [37]. We adopt the best fit

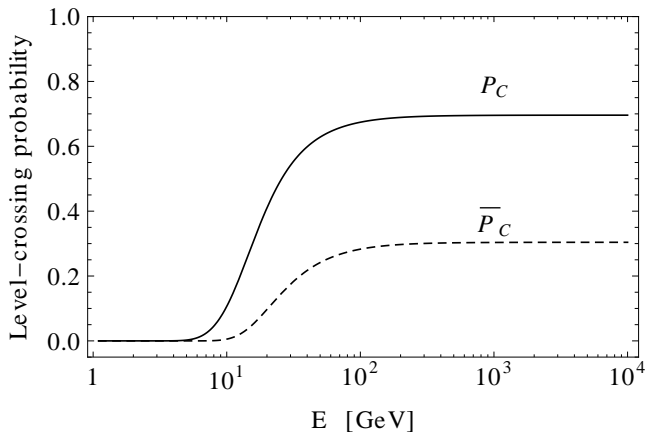


Figure 2. Level-crossing probability between mass eigenstates 1 & 2, for neutrinos (solid) and antineutrinos (dashed).

neutrino mixing parameters reported in [37–39],

$$\begin{aligned}
 \Delta m_{21}^2 &= 7.65 \times 10^{-5} \text{ eV}^2, \\
 \Delta m_{32}^2 &= 2.4 \times 10^{-3} \text{ eV}^2, \\
 \sin^2 \theta_{12} &= 0.304, \\
 \sin^2 \theta_{23} &= 0.5, \\
 \theta_{13} &= 0, \\
 \delta &= 0.
 \end{aligned}
 \tag{2.27}$$

2.3.2 $\nu_\mu - \nu_\tau$ oscillations

Muon and tau neutrinos mix maximally, and oscillate with frequency $f_{\text{osc}} = \Delta m_{32}^2/2E$. The oscillations equidistribute the neutrinos in the two flavour eigenstates, as long as f_{osc} is comparable to, or exceeds the interaction rate in the Sun, $\Gamma_{\text{int}} = \sigma_{\text{tot}}(E)N_S(r)$. In Fig. 1 we sketch the maximum energy for which

$$f_{\text{osc}} \gtrsim \Gamma_{\text{int}}, \tag{2.28}$$

as a function of the solar radius. This obtains at optical depth

$$x \gtrsim x_{\text{eq}}(E) = 1 - (\kappa R_\odot \mathcal{E} \Delta m_{32}^2) / 2E^2 \tag{2.29}$$

where we used the analytical approximation of Eq. (2.5). Although this condition is not strictly satisfied at all depths for the entire energy range of interest, it is easy to show that even the highest-energy neutrinos considered here undergo only a small number of scatterings $\lesssim 5$, before they lose enough energy and move out in radius to lower solar density, such that oscillations become more frequent than their interactions². Since the mediator decays

²On average, every NC interaction in the Sun costs neutrinos about 1/2 of their energy (CC interactions of tau neutrinos degrade their energy even more). After n interactions, the neutrino energy is diminished to $E_n \approx E_0/2^n$, and neutrinos have traversed total optical depth $\delta x_{\text{tot},n} = \delta x_0(2^{n+1} - 1)$, where $\delta x_0 = \mathcal{E}/E_0$, according to Eq. (2.20). If neutrinos are injected in the centre of the Sun, the number of scatterings they undergo till they satisfy Eq. (2.29) is found by setting $\delta x_{\text{tot},n} = x_{\text{eq}}(E_n)$. This yields $n \approx 4.6 + 3.3 \log(E_0/10 \text{ TeV})$. Neutrinos injected away from the centre undergo even less scatterings.

have been chosen to inject equal numbers of all flavours, we don't rely on the oscillations to establish the $\nu_\mu\text{-}\nu_\tau$ average as an initial condition, but only to maintain it, and thus averaging over the muon and tau neutrino populations remains an adequate approximation.

2.4 Propagation

We compare the effect of neutrino interactions and oscillations inside the Sun in Fig. 1. For all energies in the range $5 \text{ GeV} \lesssim E \lesssim 10 \text{ TeV}$, resonance between the electron and muon neutrinos occurs at $r > 0.75R_\odot$. At this region, less than 5% of the neutrinos will interact before they exit the Sun, $P_{\text{int}} < 0.05$. This allows for separate treatment of the neutrino interactions in the interior of the Sun and the neutrino resonant conversions.

We calculate the neutrino signal at the Earth according to the following procedure:

- i. We follow the evolution of the neutrino fluxes from the centre of the Sun to $r_c = 0.75R_\odot$ using Eqs. (2.4), taking into account the neutrino interactions as described in Sec. 2.2. Eqs. (2.4) are solved analytically as described below. For muon and tau neutrinos we set $\rho_{\mu,\tau} = \rho_\mu = \rho_\tau$ (and similarly for the antineutrinos), and average over their interactions. We neglect interactions at $r > r_c$, and simply add the contribution to the neutrino flux from mediator decays between r_c and the resonance point.
- ii. We evaluate the level crossings at resonance, using Eqs. (2.26). We convert the mass-eigenstate fluxes back into flavour-eigenstate ones using the standard mixing parameters given in Eq. (2.27).
- iii. We add the neutrino flux generated by decays between the point of resonance and the Earth.

We shall now describe these steps in more detail.

The evolution equations (2.4) take the form

$$\frac{\partial \rho_j}{\partial x} = h(x, E) + \frac{1}{\mathcal{E}} \left[-E \rho_j(x, E) + \int_E^\infty dE' g_j(E/E') \rho_j(x, E') \right], \quad (2.30)$$

where \mathcal{E} is given by Eqs. (2.17) and (2.18). For $r < r_c$, the exponential approximation of Eq. (2.5) for the solar profile is valid and the neutrino injection term $h(x, E)$ is expressed analytically by

$$h_a(x, E) = \frac{C_\odot \text{BR}_\nu}{\beta m_\chi} \frac{\kappa R_\odot}{\beta \gamma \tau} (1-x)^{\frac{\kappa R_\odot}{\beta \gamma \tau} - 1}, \quad (2.31)$$

for the energy interval of Eq. (2.3). The regeneration functions appearing in Eqs. (2.30) are

$$\begin{aligned} g_e(u) &= \frac{a_\nu + b_\nu u^2}{a_\nu + b_\nu/3 + c_\nu}, \\ g_{\mu,\tau}(u) &= \frac{a_\nu + b_\nu u^2 + c_\nu/2 f_{\tau \rightarrow \tau}(u)}{a_\nu + b_\nu/3 + c_\nu}, \\ g_{\bar{e}}(u) &= \frac{a_{\bar{\nu}} + b_{\bar{\nu}} u^2}{a_{\bar{\nu}} + b_{\bar{\nu}}/3 + c_{\bar{\nu}}}, \\ g_{\bar{\mu},\bar{\tau}}(u) &= \frac{a_{\bar{\nu}} + b_{\bar{\nu}} u^2 + c_{\bar{\nu}}/2 f_{\bar{\tau} \rightarrow \bar{\tau}}(u)}{a_{\bar{\nu}} + b_{\bar{\nu}}/3 + c_{\bar{\nu}}}, \end{aligned} \quad (2.32)$$

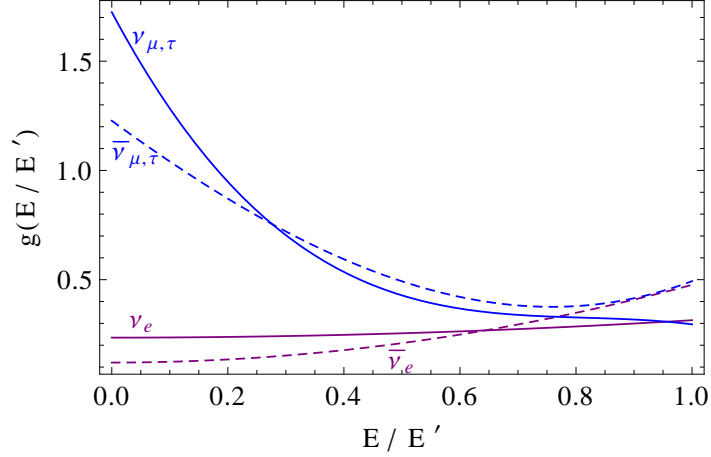


Figure 3. The regeneration functions of Eqs. (2.32), for ν_e (purple, solid), $\bar{\nu}_e$ (purple, dashed), $\nu_{\mu,\tau}$ (blue, solid), $\bar{\nu}_{\mu,\tau}$ (blue, dashed).

and are sketched in Fig. 3.

Equation (2.30) can be solved analytically for $g = 0$ and $g = 1$. For a general function g , it is possible to solve Eq. (2.30) perturbatively around these two cases. The range of values of the regeneration functions, presented in Fig. 3, renders this a suitable treatment for the neutrino propagation in the Sun. For the ν_e and $\bar{\nu}_e$ fluxes, $g_e, g_{\bar{e}} < 1$, and the perturbative solution around $g = 0$ is warranted. For the $\nu_{\mu,\tau}$ and $\bar{\nu}_{\mu,\tau}$ fluxes, the perturbative solution around $g = 1$ appears formally more appropriate. We have implemented both solutions and checked that, for the DM masses and mediator lifetimes considered here, the differences in the final spectra are small and do not qualitatively change our conclusions. For simplicity, we will thus adopt the perturbative solution around $g = 0$ for all fluxes.

The exact solution of Eq. (2.30) for $g = 0$ is

$$\rho_0(x, E) = \int_0^x dx' e^{-\frac{E(x-x')}{\mathcal{E}}} h(x', E). \quad (2.33)$$

Let

$$\rho(x, E) = \rho_0(x, E) + \rho_1(x, E), \quad (2.34)$$

where $\rho_1(x, E)$ obeys, to 1st order in g , the differential equation

$$\frac{\partial \rho_1}{\partial x} = h_1(x, E) - \frac{E}{\mathcal{E}} \rho_1(x, E), \quad (2.35)$$

with

$$h_1(x, E) \equiv \frac{1}{\mathcal{E}} \int_E^\infty dE' g(E/E') \rho_0(x, E'). \quad (2.36)$$

Eq. (2.35) has the same form as Eq. (2.30) for $g = 0$, and its solution is

$$\rho_1(x, E) = \int_0^x dx' e^{-\frac{E(x-x')}{\mathcal{E}}} h_1(x', E) \quad (2.37)$$

Eqs. (2.33), (2.34), (2.36) and (2.37) yield the perturbative solution to the evolution equation, to first order in g .

The contribution to the neutrino flux from decays of the mediators between r_c and $r_{\text{res}}(E)$ is

$$\delta\rho_{\text{I}}(E) = \frac{C_{\odot} \text{BR}_{\nu}}{\beta m_{\chi}} \left[\exp\left(-\frac{r_c}{\beta\gamma\tau}\right) - \exp\left(-\frac{r_{\text{res}}(E)}{\beta\gamma\tau}\right) \right]. \quad (2.38)$$

For $\gamma\tau \gtrsim 2$ s, the neutrino production beyond the point of resonance is significant and is given by

$$\delta\rho_{\text{II}}(E) = \frac{C_{\odot} \text{BR}_{\nu}}{\beta m_{\chi}} \left[\exp\left(-\frac{r_{\text{res}}(E)}{\beta\gamma\tau}\right) - \exp\left(-\frac{R_{\text{SE}}}{\beta\gamma\tau}\right) \right], \quad (2.39)$$

with $R_{\text{SE}} = 1$ A.U.

The final neutrino fluxes at Earth, calculated as outlined above, are presented in Figs. 4 – 8 for various choices of the DM mass and mediator lifetime, and discussed in the following section.

3 Neutrino signals

3.1 Neutrino flux results

In Figs. 4 – 8 we present the final differential neutrino fluxes at Earth, $d\Phi/dE = \rho(1\text{A.U.}, E)$, calculated as outlined in previous section, for various choices of the DM mass and mediator lifetime. All fluxes are normalised to the DM capture rate in the Sun, C_{\odot} , and the branching ratio BR_{ν} for decay to neutrinos.

In Fig. 4, we compare the ν_e fluxes obtained for different mediator lifetimes, $\gamma\tau = 0.001\text{s}, 0.1\text{s}, 0.3\text{s}, 1\text{s}, 10\text{s}$ (always assuming $\gamma \gg 1$). For small mediator lifetime, absorption effects result in an exponential suppression of the flux at high energy, while down scattering or regeneration effects cause a pile up of neutrinos at low energy. These effects can both clearly be seen in the left-hand panels of Fig. 4. Relativistic particles transverse the entire radius of the Sun in ~ 2.2 s, while the core of the Sun corresponds to $\sim 1/10$ of this distance (cf. Eq. (2.5)). Thus, the smallest mediator lifetime we consider, $\gamma\tau = 0.001$ s, effectively corresponds to the standard scenario of DM annihilation directly into SM particles in the centre of the Sun³. For the largest lifetime we consider, $\gamma\tau = 10$ s, almost all the mediators decay outside the Sun, so absorption is negligible and the characteristic flat injection spectrum of boosted 2-body decays (discussed in Sec. 2.1) is reproduced. Between these two limiting cases, the fluxes depend sensitively on the mediator lifetime.

We can quantify the degree of attenuation in terms of the neutrino injection radius as follows: if we inject all neutrinos at radius $r = r_{\text{inj}}$ and consider only absorption effects, the solution of the flux evolution equation (Eq. (2.30)) is simply

$$\rho = \rho_{\text{inj}} e^{-\frac{E}{\varepsilon} \Delta x}, \quad (3.1)$$

where ρ_{inj} is the flux at the injection radius, and Δx is the optical depth traversed. Neutrinos injected at $r = r_{\text{inj}}$ traverse an optical depth of $\Delta x = \exp\left(-\frac{r_{\text{inj}}}{\kappa R_{\odot}}\right)$ as they propagate to

³We note that the neutrino spectrum resulting from the prompt decay ($\gamma\tau \lesssim 0.2$ s, with $\gamma \gg 1$) of each metastable mediator to a neutrino pair resembles the neutrino spectrum obtained from DM annihilation to relativistic SM particles such as $\tau^+\tau^-$, rather than that for DM annihilation directly to a neutrino pair. In the latter case, neutrinos are emitted monoenergetically, which results in a residual peak in the final spectrum, at the maximum energy. In the case of decays of boosted particles, neutrinos are injected with an extended spectrum, as described in Eq. (2.3).

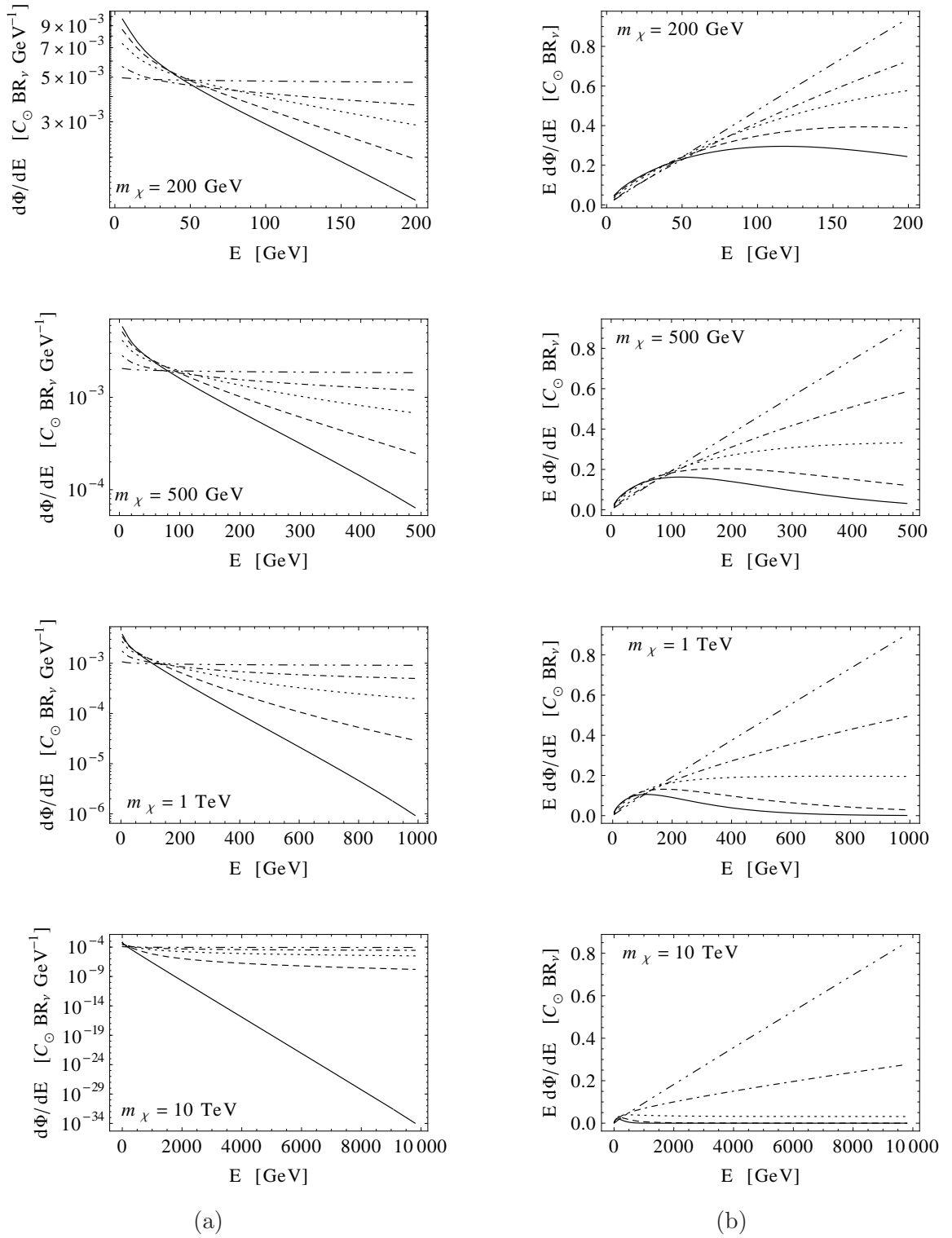


Figure 4. ν_e fluxes for $\gamma\tau = 0.001$ s (solid), 0.1 s (dashed) 0.3 s (dotted) 1 s (dot-dashed), 10 s (dot-dot-dashed), and DM masses $m_\chi = 200$ GeV (1st row), 500 GeV (2nd row), 1 TeV (3rd row), 10 TeV (4th row).

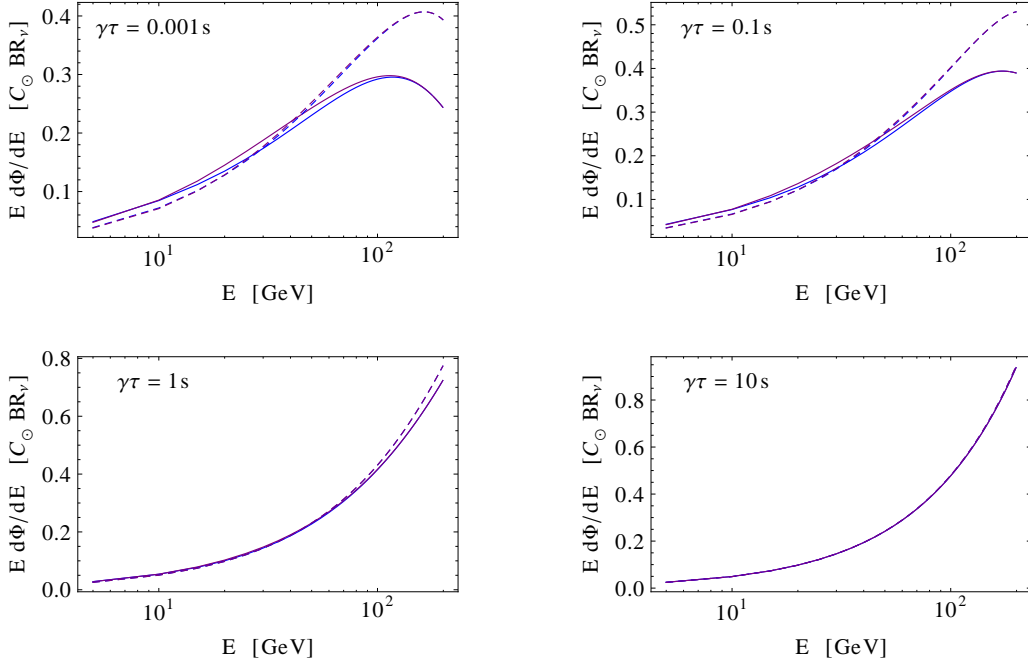


Figure 5. Neutrino fluxes at the Earth for DM mass $m_\chi = 200$ GeV, and mediator lifetimes $\gamma\tau = 0.001$ s, 0.1 s, 1 s, 10 s. In each graph the lines correspond to: ν_e flux (blue, solid), $\nu_{\mu,\tau}$ flux (purple, solid), $\bar{\nu}_e$ flux (blue, dashed), and $\bar{\nu}_{\mu,\tau}$ flux (purple, dashed).

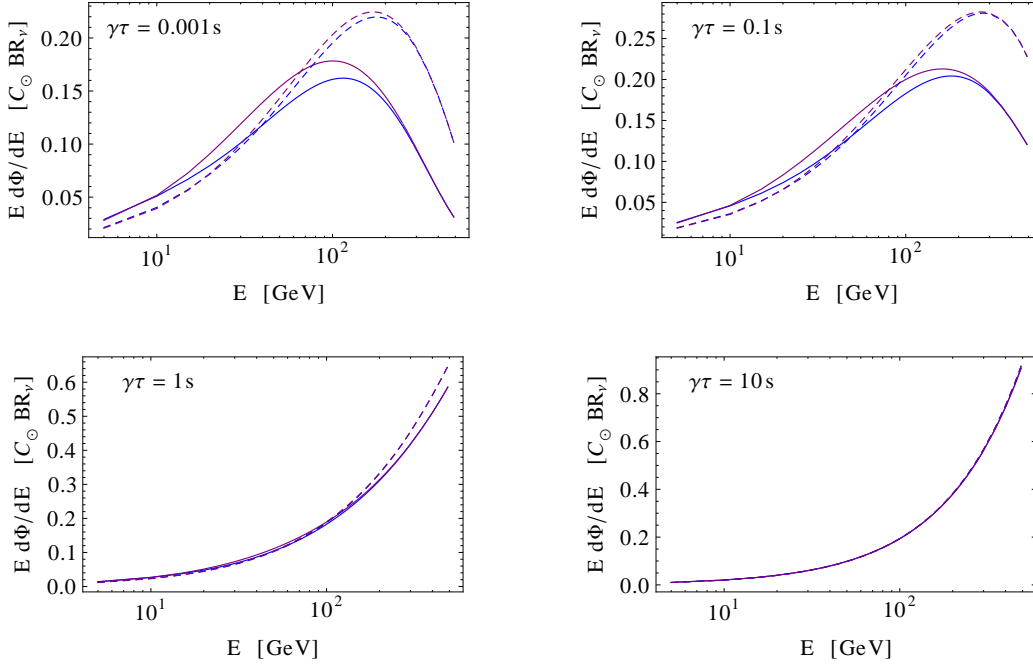


Figure 6. Same as in Fig. 5, for DM mass $m_\chi = 500$ GeV.

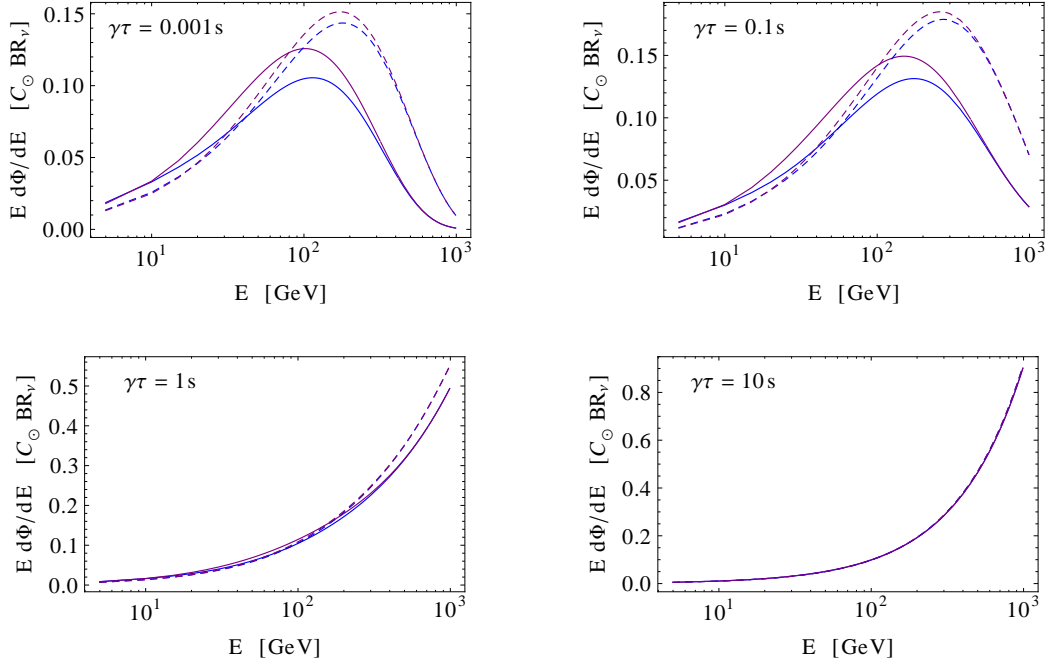


Figure 7. Same as in Fig. 5, for DM mass $m_\chi = 1 \text{ TeV}$.

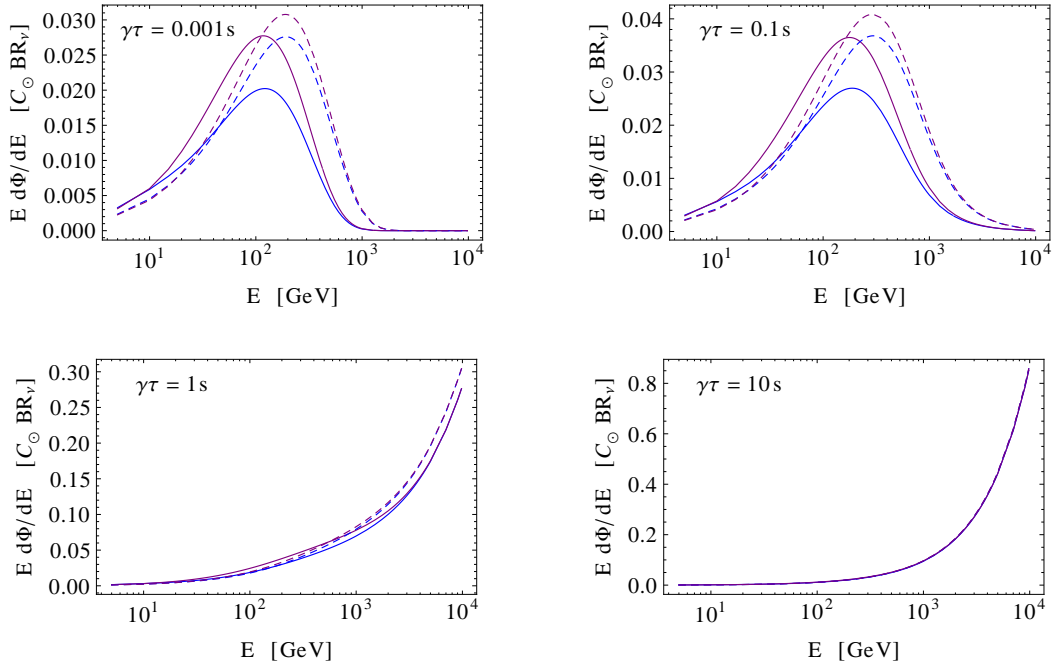


Figure 8. Same as in Fig. 5, for DM mass $m_\chi = 10 \text{ TeV}$.

$r = R_\odot$ (see Eq. (2.7)). For $r_{\text{inj}} = 0$, $\Delta x \simeq 1$, and thus $\rho = \rho_{\text{inj}} e^{-\frac{E}{\mathcal{E}'}}$. More generally, if we define a critical energy \mathcal{E}' as

$$\mathcal{E}'(r_{\text{inj}}) = \mathcal{E} \exp\left(\frac{r_{\text{inj}}}{\kappa R_\odot}\right), \quad (3.2)$$

the solution for the attenuated flux at the solar surface can be expressed as

$$\rho = \rho_{\text{inj}} e^{-\frac{E}{\mathcal{E}'}}. \quad (3.3)$$

The critical energy \mathcal{E}' controls the exponential suppression of the flux at high energies. Since \mathcal{E}' grows exponentially with injection radius, we see that this critical energy for absorption grows rapidly as soon as the injection radius is outside the core, $r_{\text{inj}} \gtrsim \kappa R_\odot$.

In the scenario considered here, mediator decays inject neutrinos not at a single point but with a distribution of radii. To account for the absorption we must employ the injection function of Eq. (2.9), or equivalently

$$\left. \frac{d\Phi}{dE} \right|_{E \gtrsim \mathcal{E}} = \frac{C_\odot \text{BR}_\nu}{\beta m_\chi} \frac{1}{\beta \gamma \tau} \int_0^\infty \exp\left(-\frac{r}{\beta \gamma \tau}\right) \exp\left(-\frac{E}{\mathcal{E}'(r)}\right) dr. \quad (3.4)$$

This provides a good approximation for the flux for high energies $E \gtrsim \mathcal{E}$, where absorption is the leading effect. Regeneration effects become relevant at lower energies, where a pile up of low energy neutrinos enhances the fluxes above the levels indicated by Eq. (3.4).

Annihilation via the mediators enhances the prospects for detection of a DM annihilation signal from the Sun. In the right-hand panels of Fig. 4 (and in Figs. 5 – 8) we plot the quantity $E d\Phi/dE$. As the neutrino scattering cross-section on nucleons is proportional to the energy (see Eq. (2.19)), the area under the $E d\Phi/dE$ vs. E graphs is a guide to the relative event rates in neutrino detector. For all DM masses and mediator lifetimes, the prospects for detection are better at neutrino energies $E_\nu \gtrsim 100$ GeV, and dramatically so as the DM mass is increased. Since the high energy neutrinos are the most enhanced and also have the largest detection cross sections, the mediator scenario is particularly effective in enhancing event rates.

The neutrino spectral shape is a striking signature of DM annihilation via metastable states. In the standard scenario, there is never significant neutrino flux at energies $E_\nu \gtrsim 1$ TeV. If DM annihilates directly into SM particles, $E d\Phi/dE$ exhibits a peak around ~ 100 GeV (see Figs. 5 – 8). The peak occurs because the absorption increases strongly with energy and always quells the spectrum at higher energies. In fact, for $m_\chi > 1$ TeV, neutrino interactions in the Sun drive the spectrum to a fixed shape independent of the DM mass or annihilation channel (dubbed the “limit spectrum” in Ref. [3]) with a sharp cutoff at $E_\nu \approx 1$ TeV. These features are reproduced by our calculations for $\gamma\tau = 0.001$ s. In the presence of mediators, however, the peak of the spectrum moves to higher energy if $\gamma\tau$ is small, and completely disappears for $\gamma\tau \gtrsim 0.3$ s (which corresponds to mediator decay outside the core of the Sun). Although the small shift in the spectral shape for small $\gamma\tau$ may not be readily discernible, the rising trend of the spectrum ($E d\Phi/dE$) at high energies that occurs in the case of sufficiently long-lived mediators is a firm signature of this scenario. It cannot arise in the standard scenario, even for very large DM mass. A potential observation of a neutrino signal from the Sun at energies $E_\nu \gtrsim 1$ TeV can thus be justified only in the context of DM annihilation into metastable states with $\gamma\tau > 0.1$ s.

We compare the fluxes of all neutrinos flavours, for both neutrinos and antineutrinos, in Figs. 5 – 8. We have assumed that the mediators decay with equal branching ratio to

all flavours. However, interactions induce flux differences between neutrinos and antineutrinos, and between the different flavours. Neutrinos interact more strongly in the Sun than antineutrinos, thus are absorbed more, resulting in smaller fluxes. Due to the ν_τ and $\bar{\nu}_\tau$ regeneration, the muon/tau neutrino and antineutrino fluxes are higher than the electron-type ones. These features are more apparent for larger DM masses and smaller mediator lifetimes, when interactions are stronger. As the mediator lifetime is increased, such that interactions become less important, the spectra for all flavours of ν and $\bar{\nu}$ merge.

3.2 Muon event rates

We shall now estimate the number of muon track events in the IceCube detector for a range of mediator lifetimes, relative to the scenario in which the neutrinos are produced in the solar core. We estimate event rates following the procedure in Refs. [40–42], which is outlined below.

A muon neutrino of energy E produces a muon with energy $E_\mu = E(1 - y)$ when it undergoes a charged current interaction, where y is the charged current inelasticity parameter. For simplicity we will adopt the mean values of y tabulated in Ref. [40], which are approximately ~ 0.45 for neutrinos and ~ 0.35 for antineutrinos. Muons propagate over a long distance before they decay, such that IceCube can detect muons created from ν_μ interactions well outside the detector. The muons lose energy as they propagate, and have a range given by

$$R_\mu(E_\mu, E_\mu^{\text{thr}}) = \frac{1}{\beta} \ln \left[\frac{\alpha + \beta E_\mu}{\alpha + \beta E_\mu^{\text{thr}}} \right], \quad (3.5)$$

where $\alpha = 2.0 \text{ MeV cm}^2/\text{g}$, $\beta = 4.2 \times 10^{-6} \text{ cm}^2/\text{g}$, and E_μ^{thr} is the muon energy detection threshold for the detector (see, e.g., Refs. [40–43]). We will take E_μ^{thr} to be 100 GeV. The probability that a neutrino of energy E makes a muon track that is detected with energy above E_μ^{thr} is then

$$P(E, E_\mu^{\text{thr}}) = \rho_N N_A \sigma_{\text{nucleon}} R_\mu(E(1 - y), E_\mu^{\text{thr}}), \quad (3.6)$$

where ρ_N is the target nucleon density and N_A is Avogadro’s number. The muon track event rate is thus proportional to

$$\int \frac{d\Phi(E)}{dE} P(E, E_\mu^{\text{thr}}) A^{\text{eff}} dE \quad (3.7)$$

where A^{eff} is the effective area of the detector, which is $\sim 1 \text{ km}^2$ for IceCube [44].

In table 1, we show the relative number of muon track events for different choices of the mediator lifetime, normalised to the case where $\tau \simeq 0$ (i.e., production in the centre of the Sun). For the latter, we adopt the fluxes obtained here for $\gamma\tau = 0.001 \text{ s}$, in order to retain consistency with our calculations. Both neutrino and antineutrino events are included, weighted according to their respective CC interaction probabilities (which have a ratio of approximately 2:1 in ice). For dark matter masses close the transparency energy of the Sun $\sim 200 \text{ GeV}$, the effect of the metastable mediator is to enhance the flux by about a factor 2. For larger dark matter masses, well above the energy at which the Sun becomes opaque neutrinos, annihilation via metastable mediators has a huge effect on the flux, with an enhancement of an order of magnitude for lifetime as short as 0.1s, and an enhancement of about 1000 for lifetime comparable to the solar radius. Particularly for these heavy dark matter masses, the presence of the metastable mediator greatly enhances the flux which emerges from the Sun, and therefore the detection prospects.

	200 GeV	500 GeV	1 TeV	10 TeV
0.1 s	1.4	1.9	2.9	1.2×10
0.3 s	1.9	3.4	7.6	2.7×10^2
1s	2.3	4.8	1.4×10	1.4×10^3
10 s	2.9	6.7	2.2×10	3.6×10^3

Table 1. The ratio of μ^\pm events observable in the presence of mediators of lifetime $\gamma\tau$ over those in the absence of metastable mediators, $\Phi(\gamma\tau)/\Phi(\gamma\tau \rightarrow 0)$, integrated over muon energies $E_\mu > 100\text{GeV}$, for various dark-matter masses and mediator lifetimes. We have used the calculated fluxes from our analysis for $\gamma\tau = 0.001\text{ s}$ as the benchmark fluxes for DM annihilation directly into SM particles.

4 Conclusions

The search for high energy neutrinos produced by the annihilation of DM captured in the Sun is a promising means of indirect DM detection. A future detection can provide information about the DM annihilation channels, which is critical for the identification of the particle nature of DM. It is possible, however, that DM does not annihilate directly into SM particles. We have examined a scenario in which DM annihilates to metastable mediators, which subsequently decay to SM states. In these models, though the DM and SM sectors are secluded from each other and communicate only via the mediators, the standard thermal-WIMP scenario can be realised as usual. Existing DM indirect detection bounds are modified in these models. Particularly interesting is the signal from DM capture in the Sun, which is enhanced at high energy and provides distinct features which can unmask the secluded nature of DM.

In the case where the mediators propagate out from the dense solar core before decaying, the neutrinos produced in the decays experience a much smaller optical depth and thus much less absorption, compared to neutrino production at the centre of the Sun. In the standard scenario, the absorption is so severe that the flux is almost completely suppressed beyond about 1 TeV. The observation of a solar neutrino flux beyond 1 TeV would thus be striking indication of the presence of metastable mediators. These features would be discernible even with small number of events, or poor detector energy resolution, and remain valid independent of the specific decay channel of the mediators into SM states. Finally, this enhancement of the neutrino flux at high energy is particularly effective in improving detection prospects, given that the detection cross sections grow with energy.

Acknowledgments

We thank John Beacom for helpful discussions. This work was supported, in part, by the Australian Research Council.

References

- [1] W. H. Press and D. N. Spergel, *Capture by the sun of a galactic population of weakly interacting, massive particles*, *Astrophys. J.* **296** (1985) 679–684.
- [2] A. Gould, *Resonant Enhancements in WIMP Capture by the Earth*, *Astrophys. J.* **321** (1987) 571.

- [3] M. Cirelli *et. al.*, *Spectra of neutrinos from dark matter annihilations*, *Nucl. Phys.* **B727** (2005) 99–138, [[hep-ph/0506298](#)].
- [4] M. Blennow, J. Edsjo, and T. Ohlsson, *Neutrinos from WIMP Annihilations Using a Full Three-Flavor Monte Carlo*, *JCAP* **0801** (2008) 021, [[arXiv:0709.3898](#)].
- [5] M. Kamionkowski, *Energetic neutrinos from heavy neutralino annihilation in the sun*, *Phys. Rev.* **D44** (1991) 3021–3042.
- [6] P. Crotty, *High-energy neutrino fluxes from supermassive dark matter*, *Phys. Rev.* **D66** (2002) 063504, [[hep-ph/0205116](#)].
- [7] H. Baer, A. Belyaev, T. Krupovnickas, and J. O’Farrill, *Indirect, direct and collider detection of neutralino dark matter*, *JCAP* **0408** (2004) 005, [[hep-ph/0405210](#)].
- [8] V. D. Barger, F. Halzen, D. Hooper, and C. Kao, *Indirect search for neutralino dark matter with high energy neutrinos*, *Phys. Rev.* **D65** (2002) 075022, [[hep-ph/0105182](#)].
- [9] V. Berezhinsky *et. al.*, *Searching for relic neutralinos using neutrino telescopes*, *Astropart. Phys.* **5** (1996) 333–352, [[hep-ph/9603342](#)].
- [10] L. Bergstrom, J. Edsjo, and P. Gondolo, *Indirect neutralino detection rates in neutrino telescopes*, *Phys. Rev.* **D55** (1997) 1765–1770, [[hep-ph/9607237](#)].
- [11] L. Bergstrom, J. Edsjo, and P. Gondolo, *Indirect detection of dark matter in km-size neutrino telescopes*, *Phys. Rev.* **D58** (1998) 103519, [[hep-ph/9806293](#)].
- [12] L. Bergstrom, J. Edsjo, and M. Kamionkowski, *Astrophysical-neutrino detection with angular and energy resolution*, *Astropart. Phys.* **7** (1997) 147–160, [[astro-ph/9702037](#)].
- [13] V. Bertin, E. Nezri, and J. Orloff, *Neutrino indirect detection of neutralino dark matter in the CMSSM*, *Eur. Phys. J.* **C26** (2002) 111–124, [[hep-ph/0204135](#)].
- [14] V. Bertin, E. Nezri, and J. Orloff, *Neutralino dark matter beyond CMSSM universality*, *JHEP* **02** (2003) 046, [[hep-ph/0210034](#)].
- [15] A. Bottino, V. de Alfaro, N. Fornengo, G. Mignola, and M. Pignone, *Indirect search for neutralinos at neutrino telescopes*, *Phys. Lett.* **B265** (1991) 57–63.
- [16] A. Bottino, F. Donato, N. Fornengo, and S. Scopel, *Combining the data of annual modulation effect in WIMP direct detection with measurements of WIMP indirect searches*, *Astropart. Phys.* **10** (1999) 203–210, [[hep-ph/9809239](#)].
- [17] A. E. Faraggi, K. A. Olive, and M. Pospelov, *Probing the desert with ultra-energetic neutrinos from the sun*, *Astropart. Phys.* **13** (2000) 31–43, [[hep-ph/9906345](#)].
- [18] J. L. Feng, K. T. Matchev, and F. Wilczek, *Prospects for indirect detection of neutralino dark matter*, *Phys. Rev.* **D63** (2001) 045024, [[astro-ph/0008115](#)].
- [19] G. B. Gelmini, P. Gondolo, and E. Roulet, *Neutralino dark matter searches*, *Nucl. Phys.* **B351** (1991) 623–644.
- [20] F. Halzen, T. Stelzer, and M. Kamionkowski, *Signatures of dark matter in underground detectors*, *Phys. Rev.* **D45** (1992) 4439–4442.
- [21] **Super-Kamiokande** Collaboration, S. Desai *et. al.*, *Search for dark matter WIMPs using upward through-going muons in Super-Kamiokande*, *Phys. Rev.* **D70** (2004) 083523, [[hep-ex/0404025](#)].
- [22] **ICECUBE** Collaboration, R. Abbasi *et. al.*, *Limits on a muon flux from neutralino annihilations in the Sun with the IceCube 22-string detector*, *Phys. Rev. Lett.* **102** (2009) 201302, [[arXiv:0902.2460](#)].
- [23] **The IceCube** Collaboration, R. Abbasi *et. al.*, *Limits on a muon flux from Kaluza-Klein dark matter annihilations in the Sun from the IceCube 22-string detector*, *Phys. Rev.* **D81** (2010)

- 057101, [[arXiv:0910.4480](#)].
- [24] M. Pospelov, A. Ritz, and M. B. Voloshin, *Secluded WIMP Dark Matter*, *Phys. Lett.* **B662** (2008) 53–61, [[arXiv:0711.4866](#)].
- [25] D. P. Finkbeiner and N. Weiner, *Exciting Dark Matter and the INTEGRAL/SPI 511 keV signal*, *Phys. Rev.* **D76** (2007) 083519, [[astro-ph/0702587](#)].
- [26] N. Arkani-Hamed, D. P. Finkbeiner, T. R. Slatyer, and N. Weiner, *A Theory of Dark Matter*, *Phys. Rev.* **D79** (2009) 015014, [[arXiv:0810.0713](#)].
- [27] M. Pospelov and A. Ritz, *Astrophysical Signatures of Secluded Dark Matter*, *Phys. Lett.* **B671** (2009) 391–397, [[arXiv:0810.1502](#)].
- [28] I. Z. Rothstein, T. Schwetz, and J. Zupan, *Phenomenology of Dark Matter annihilation into a long-lived intermediate state*, *JCAP* **0907** (2009) 018, [[arXiv:0903.3116](#)].
- [29] F. Chen, J. M. Cline, and A. R. Frey, *Nonabelian dark matter: models and constraints*, *Phys. Rev.* **D80** (2009) 083516, [[arXiv:0907.4746](#)].
- [30] B. Batell, M. Pospelov, A. Ritz, and Y. Shang, *Solar Gamma Rays Powered by Secluded Dark Matter*, *Phys. Rev.* **D81** (2010) 075004, [[arXiv:0910.1567](#)].
- [31] P. Schuster, N. Toro, N. Weiner, and I. Yavin, *High Energy Electron Signals from Dark Matter Annihilation in the Sun*, *Phys.Rev.* **D82** (2010) 115012, [[arXiv:0910.1839](#)].
- [32] J. N. Bahcall, A. M. Serenelli, and S. Basu, *New solar opacities, abundances, helioseismology, and neutrino fluxes*, *Astrophys. J.* **621** (2005) L85–L88, [[astro-ph/0412440](#)].
- [33] R. Gandhi, C. Quigg, M. H. Reno, and I. Sarcevic, *Neutrino interactions at ultrahigh-energies*, *Phys. Rev.* **D58** (1998) 093009, [[hep-ph/9807264](#)].
- [34] S. I. Dutta, M. H. Reno, and I. Sarcevic, *Secondary neutrinos from tau neutrino interactions in earth*, *Phys. Rev.* **D66** (2002) 077302, [[hep-ph/0207344](#)].
- [35] A. Cooper-Sarkar and S. Sarkar, *Predictions for high energy neutrino cross-sections from the ZEUS global PDF fits*, *JHEP* **0801** (2008) 075, [[arXiv:0710.5303](#)].
- [36] A. Strumia and F. Vissani, *Neutrino masses and mixings and..*, [[hep-ph/0606054](#)].
- [37] **Particle Data Group** Collaboration, K. Nakamura *et. al.*, *Review of particle physics*, *J. Phys.* **G37** (2010) 075021.
- [38] G. Fogli, E. Lisi, A. Marrone, A. Melchiorri, A. Palazzo, *et. al.*, *Observables sensitive to absolute neutrino masses. 2.*, *Phys.Rev.* **D78** (2008) 033010, [[arXiv:0805.2517](#)].
- [39] T. Schwetz, M. Tortola, and J. W. Valle, *Three-flavour neutrino oscillation update*, *New J.Phys.* **10** (2008) 113011, [[arXiv:0808.2016](#)].
- [40] R. Gandhi, C. Quigg, M. H. Reno, and I. Sarcevic, *Ultrahigh-energy neutrino interactions*, *Astropart.Phys.* **5** (1996) 81–110, [[hep-ph/9512364](#)].
- [41] S. Dutta, M. Reno, I. Sarcevic, and D. Seckel, *Propagation of muons and taus at high-energies*, *Phys.Rev.* **D63** (2001) 094020, [[hep-ph/0012350](#)].
- [42] J. F. Beacom, N. F. Bell, D. Hooper, S. Pakvasa, and T. J. Weiler, *Measuring flavor ratios of high-energy astrophysical neutrinos*, *Phys.Rev.* **D68** (2003) 093005, [[hep-ph/0307025](#)].
- [43] D. E. Groom, N. V. Mokhov, and S. I. Striganov, *Muon stopping power and range tables 10-MeV to 100-TeV*, *Atom.Data Nucl.Data Tabl.* **78** (2001) 183–356.
- [44] **IceCube** Collaboration, J. Ahrens *et. al.*, *Sensitivity of the IceCube detector to astrophysical sources of high energy muon neutrinos*, *Astropart. Phys.* **20** (2004) 507–532, [[astro-ph/0305196](#)].